Available online at www.sciencedirect.com
SCIENCE DIRECT
ELSEVIER
European Journal of Mechanics B/Fluids 24 (2005) 149–165
EUROPEAN JOURNAL OF MECHANICS B/FLUIDS

Shaping of sessile liquid metal drops using high-frequency magnetic fields

Michael Conrath *, Christian Karcher

Department of Mechanical Engineering, Technische Universität Ilmenau, PO Box 100565, 98684 Ilmenau, Germany

Received 5 January 2004; received in revised form 15 April 2004; accepted 15 June 2004

Available online 10 August 2004

Abstract

An analytical model for the electromagnetic shaping of sessile liquid metal drops in high-frequency magnetic fields is presented. We deal with both an infinitely long drop and a circular drop. In each case, the arrangement of drop and inductor is symmetric. Applying the skin depth approximation reduces the Lorentz forces induced in the liquid metal drop to a magnetic pressure on the drop surface. We neglect the coupling between drop contour and magnetic field distribution. In this case, the magnetic field can be calculated analytically applying the mirror-current method. Finally, we achieve an analytical solution of the static drop contours with the help of Green's functions. The theory is applied to three problems: (i) squeezing a drop while conserving its volume, (ii) drops with a fixed contact line, (iii) pumping up of drops. The results demonstrate the suitability of high-frequency magnetic fields for the shaping of liquid metals.

Keywords: Liquid metal; Free surface; Alternating magnetic field; Electromagnetic casting; Sessile drop

1. Introduction

Metallurgical applications increasingly involve magnetic fields. Via the Lorentz forces, induced in the electrically conducting liquid, they allow contactless heating and controlling of chemically aggressive, hot melts. Common applications include induction heating, electromagnetic stirring and pumping, and affecting liquid metal jets while pouring (Davidson [1]). Another application of magnetic fields is electromagnetic shaping. In this case, the induced Lorentz forces are used to control the free surface of liquid melts. Examples are cold-crucible technologies (Tanado [2]) and semi-levitation (Takeuchi [3]). Here, the idea is to prevent intense contact between the melt and crucible material. For example, Evans et al. [4] describe the production of a metal column which is slowly moving downward while the melt, held by electromagnetic forces, flows onto its top and solidifies. A similar procedure for electron beam evaporation is proposed by Kocourek et al. [5]. In this case, the solid metal column moves upward. On the top it is molten and then evaporated by an electron beam. A high-frequency magnetic field prevents the hot melt from draining.

Motivated by these potential applications, we investigate the behavior of liquid metal drops in high-frequency magnetic fields. Molokov and Reed [6] study free surface melt flows in static magnetic fields theoretically using an asymptotical method for strong magnetic fields. They consider a drop-shaped rivulet flowing down an inclined plane and submitted to a strong

* Corresponding author. Tel.: +49-3677-692465; fax: +49-3677-691281.
E-mail address: michael.conrath@tu-ilmenau.de (M. Conrath).

0997-7546/$ – see front matter
doi:10.1016/j.euromechflu.2004.06.005

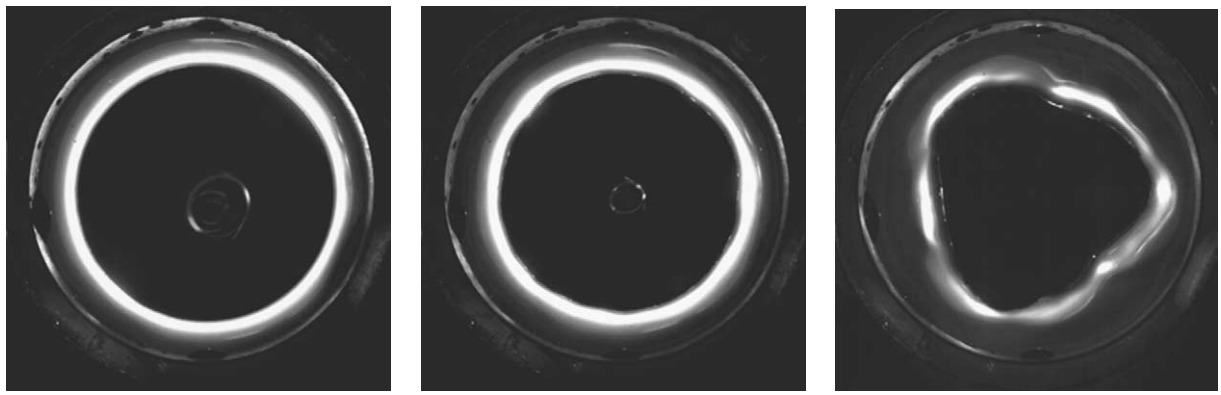

(a) (b) (c)

Fig. 1. Experimental observation of a liquid metal drop affected by a high-frequency magnetic field. (a) Static drop shape in the absence of the magnetic field ($I = 0$), (b) static drop shape in the presence of a magnetic field at $I = 80$ A and $f = 20$ KHz, (c) dynamic drop shape in the presence of a magnetic field at $I = 150$ A and $f = 20$ KHz. The drop slowly oscillates with a frequency in the range of $f = 2$–3 Hz and a mode number $m = 3$.

magnetic field perpendicular to flow direction. The magnetic field is directed normal as well as tangential to the plane. In their theory, the contact angle is assumed to be fixed as no experimental data is available describing the contact angle dynamics in magnetic fields. For magnetic fields normal to the plane, the flow inside the rivulet is determined by an equilibrium of Lorentz forces and gravity. At the bottom, a thin Hartmann boundary layer is built up which reduces the flow velocity. In the case of a horizontal magnetic field, gravity is balanced by friction forces. The flow velocity is independent of the magnetic field strength. Fautrelle et al. [7] studied the dynamic behavior of liquid metal drops in low-frequency magnetic fields. The applied frequencies are of a few hertz, corresponding to the eigenfrequencies of a spherical drop (Landau and Lifschitz [8]). The analysis shows that resonance effects occur, i.e. the frequency of the generated surface wave is a multiple of the exciting frequency. In the present paper we focus on electromagnetic shaping of liquid metal drops using fields of high frequency of some kilohertz. Due to the skin effect (Jackson [9]), the induced Lorentz forces then act like an additional pressure on the free surface of the drop. For example, this effect is also used by Riahi and Walker [10] as well as Lie et al. [11] who tackle the problem of float zone shaping in silicon crystal growth using radio frequency of about $f = 3$ MHz.

In our case, accompanying experiments [12] indicate the drop dynamics. Figs. 1(a)–(c) show contours of a liquid drop of the low-melting metal Galinstan, photographed from above. The drop volume remains $V = 7$ ml in all three pictures. Fig. 1(a) shows the circular contour of the drop in the absence of a magnetic field. Fig. 1(b) shows the drop contour when submitted to a high frequency magnetic field. The field is generated by a circular inductor fed by an alternating current of $I = 80$ A and $f = 20$ kHz. Although a weak undulating is observed, the drop retains its circular shape. Moreover, the circumference is reduced. However, on increasing the inductor current beyond a critical value, the circular shape becomes unstable, see Fig. 1(c). For $I = 150$ A and $f = 20$ kHz the drop oscillates slowly (2–3 Hz) around its equilibrium shape with a mode number depending on drop volume. The analytical model described in this paper predicts the static deformation of liquid metal drops in high-frequency magnetic fields. For simplification, the analysis is restricted to flat drops with fixed contact angle. We consider infinitely long drops as well as circular drops. In both cases, we focus on a symmetrical arrangement to obtain a two-dimensional problem.

The paper is organized as follows. In Section 2 we present the analytical model. We derive an inhomogeneous differential equation that describes the static shape of the drop. Restricting the analysis to flat drops, we achieve a solution using Green's function theory. In Section 3 we show the main results of our analysis. Three types of shaping problems are discussed: (i) squeezing of a drop, (ii) the static equilibrium shapes of drops with fixed contact line, (iii) the pumping up of a drop in an applied field. Section 4 provides a short summary.

2. Analytical model

2.1. Description of the arrangement

Fig. 2 shows a sketch of the long drop (Fig. 2(a)) as well as the circular drop (Fig. 2(b)). While the long drop is described in a Cartesian x–z-plane, cylindrical coordinates r–z are used for the circular drop. The drop is placed on an electrically conducting ground plate at $z = 0$. The drop contour is given by $h(x)$ for the long drop and $h(r)$ for the circular drop. The contour touches

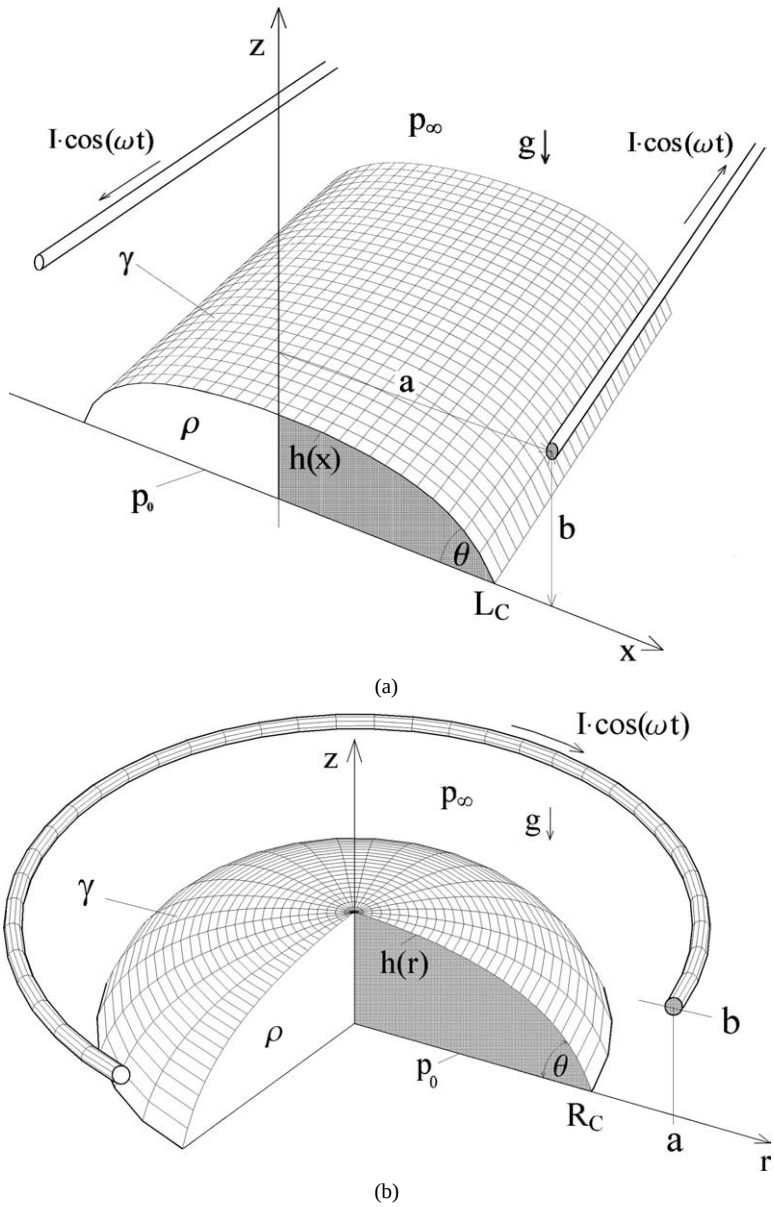

Fig. 2. Properties of drop and corresponding inductor under investigation. (a) mirrorsymmetric arrangement due to the infinitely long drop, (b) axisymmetric arrangement due to the circular drop.

the ground with a contact angle θ. The contact line is located at $x = L_C$ and $r = R_C$, respectively. The constant fluid properties are the density ρ and the surface tension γ. The ambient pressure is p_∞, while the pressure inside the drop on the bottom is p_0. Gravity g acts downward. The magnetic field is generated by an inductor filament symmetrically positioned at height $z = b$ above the plate and at distance $x = a$ and $r = a$, respectively, to the center of symmetry. The inductor is fed by an alternating electrical current $I \cdot \cos(\omega t)$ of frequency ω.

We shall treat both arrangements simultaneously. Equations related to the long drop will be indicated by an "L", while those of the circular drop are indicated by a "C". This distinction will be skipped for equations that are valid for both drops.

2.2. Assumptions

Skin depth approximation. Due to the so-called skin effect, high-frequency magnetic fields cannot penetrate an electrically conducting material. The effects are restricted to a thin layer of thickness

$$\delta = \sqrt{2/(\omega\sigma\mu)}, \tag{1}$$

the so-called equivalent skin depth (see for example Jackson [9]). Here, σ and μ are the electrical conductivity and the magnetic permeability, respectively. We assume that the skin depth is very small compared to the characteristic length scale, i.e. we consider the limit $\delta/L_{C0} \to 0$. Within this limit, the induced Lorentz forces act in a very thin layer to the surface, corresponding to a magnetic (Moreau [13]) on the drop surface. The magnetic pressure is defined by the relation

$$p_M = B_S^2/2\mu, \tag{2}$$

where B_S is the tangential component of the magnetic field on the surface. According to Eq. (1) the skin depth approximation is justified for high inductor frequencies and high electrical conductivities. Both requirements are met in the present problem.

Flat drop approximation. Furthermore, to simplify the problem we restrict the analysis to flat drops. In this case, the slope of the drop contour is assumed to be small, i.e.

$$h' \ll 1. \tag{3}$$

To estimate the validity of this approximation we compare the purely hydrostatic ($p_M \equiv 0$) drop contours of approximated (cf. Eq. (8)) and exact solution (cf. Eq. (7)). The approximated solutions show deviations less than 10% from the exact solutions up to a contact angle of $\theta = 30°$. In the present analysis we shall assume that θ is fixed.

Mirror image method. Within the limit of the skin depth approximation, no magnetic field will penetrate into the electrically conducting ground plate. Thus, for an infinitely extended plate, the magnetic field in absence of the drop can be calculated analytically using the mirror image method (see Jackson [9]). We assume that the flat drop merely affects the magnetic field distribution of Fig. 1. This assumption is justified in the limit

$$h(0)/b \ll 1. \tag{4}$$

This limit allows us to apply the magnetic field calculated at $z = 0$ on the drop surface at $z = h$. In doing so we shall find an analytic expression for the magnetic pressure, cf. Eq. (2).

2.3. Static pressure equilibrium

The static pressure equilibrium on the drop surface at $z = h$ is given by the relation

$$(p_0 - \rho g h) - p_\infty = -\gamma k_1 + p_M, \tag{5L}$$

$$(p_0 - \rho g h) - p_\infty = -\gamma (k_1 + k_2) + p_M. \tag{5C}$$

Physically, Eqs. (5) denote that the pressure jump at the interface is balanced by both surface tension and magnetic pressure. Here k_1 and k_2 represent the main curvatures of the surface, defined by

$$k_1 = h''\left(1 + h'^2\right)^{-3/2}, \tag{6L}$$

$$k_1 + k_2 = h''\left(1 + h'^2\right)^{-3/2} + h'\left\{r\left(1 + h'^2\right)^{1/2}\right\}^{-1}, \tag{6C}$$

where the prime indicates a derivate with respect to x and r. Substituting Eqs. (6) into Eqs. (5) yields the so-called Young–Laplace equations [14,15]

$$\frac{h''}{(1 + h'^2)^{3/2}} - \frac{\rho g}{\gamma} h = \frac{p_\infty - p_0}{\gamma} + \frac{p_M(x)}{\gamma}, \tag{7L}$$

$$\frac{h''}{(1 + h'^2)^{3/2}} + \frac{h'}{r(1 + h'^2)^{1/2}} - \frac{\rho g}{\gamma} h = \frac{p_\infty - p_0}{\gamma} + \frac{p_M(r)}{\gamma}. \tag{7C}$$

Upon applying the flat drop approximation, i.e. the assumption $h' \ll 1$, we obtain the linear equations

$$h'' - \frac{\rho g}{\gamma} h = \frac{p_\infty - p_0}{\gamma} + \frac{p_M(x)}{\gamma}, \tag{8L}$$

$$h'' + \frac{1}{r} h' - \frac{\rho g}{\gamma} h = \frac{p_\infty - p_0}{\gamma} + \frac{p_M(r)}{\gamma}. \tag{8C}$$

It is convenient to nondimensionalize these equations. As an appropriate length scale we introduce the contact length in absence of the magnetic field, L_{C0} and R_{C0}, respectively. According to Eq. (2), the magnetic pressure is scaled by $p_M \propto B_0^2/(2\mu)$ where B_0 denotes a characteristic magnetic induction. We obtain

$$h'' - Bo\,h = \kappa + \kappa_M f_1(x), \tag{9L}$$

$$h'' + \frac{1}{r}h' - Bo\,h = \kappa + \kappa_M f_1(r). \tag{9C}$$

In Eqs. (9) we identify three parameters, namely the Bond number *Bo*, the pressure ratio κ, and the magnetic pressure ratio κ_M defined by

$$Bo = \frac{\rho g L_{C0}^2}{\gamma}, \tag{10L}$$

$$Bo = \frac{\rho g R_{C0}^2}{\gamma}, \tag{10C}$$

$$\kappa = \frac{(p_\infty - p_0)L_{C0}}{\gamma}, \tag{11L}$$

$$\kappa = \frac{(p_\infty - p_0)R_{C0}}{\gamma}, \tag{11C}$$

$$\kappa_M = \frac{B_0^2 L_{C0}}{2\mu\gamma}, \tag{12L}$$

$$\kappa_M = \frac{B_0^2 R_{C0}}{2\mu\gamma}. \tag{12C}$$

They represent the ratio of hydrostatic pressure, pressure difference and magnetic pressure to the surface tension pressure, respectively. Here $f_1(x)$ and $f_1(r)$ denote functions of order one representing the horizontal distribution of the magnetic pressure. The boundary and symmetry conditions to Eqs. (9) read as

$$h(x=1)=0, \qquad h'(x=0)=0, \qquad h'(x=1)=\tan\theta, \tag{13L}$$

$$h(r=1)=0, \qquad h'(r=0)=0, \qquad h'(r=1)=\tan\theta. \tag{13C}$$

2.4. Magnetic pressure on the drop surface

To close the problem given by Eqs. (9) it is necessary to derive an analytical expression for the distribution of the magnetic pressure. As mentioned before, in the double limit $\delta/L_{C0} \to 0$ and $h(0)/b \ll 1$, the mirror image method can be applied. Fig. 3 illustrates this method for the Cartesian case. The two real inductor filaments at $z = b$ are supplemented by mirror filaments at $z = -b$ that are fed by a current of the same magnitude but of opposite direction. It is obvious that in such an arrangement only the tangential component of the magnetic field contributes to the magnetic pressure. The axisymmetric analogy is given by a circular current loop reflected at $z = 0$, see Smythe [16]. The magnetic field can be easily calculated by applying the Biot–Savart law (see Jackson [9]) to the present geometric arrangement. After some straightforward analysis we obtain

$$B_x(z=0) = 2B_0\left[\frac{(b/a)}{(b/a)^2+(x/a+1)^2} - \frac{(b/a)}{(b/a)^2+(x/a-1)^2}\right], \tag{14L}$$

$$B_r(z=0) = B_0\frac{b\sqrt{a}}{2r\sqrt{r}}k\left[\frac{2+k^2}{2}K\left(k^2\right) - \frac{1}{1-k^2}E\left(k^2\right)\right], \tag{14C}$$

where in Eq. (14C) K and E represent the complete elliptic integrals of the first and second kind, respectively. The parameter k is defined as $k^2 = 4ra[(r+a)^2+b^2]^{-1}$, and $B_0 = \mu I/(2\pi a L_{C0})$ and $B_0 = \mu I/(2\pi a R_{C0})$ denote the characteristic flux densities for each case. For the distribution function of the magnetic pressure at $z = 0$ we find

$$f_1(x) = 4\left[\frac{(b/a)}{(b/a)^2+(x/a+1)^2} - \frac{(b/a)}{(b/a)^2+(x/a-1)^2}\right]^2, \tag{15L}$$

$$f_1(r) = \frac{4b^2}{r^2[(r+a)^2+b^2]}\left[\frac{2+k^2}{2}\cdot K\left(k^2\right) - \frac{1}{1-k^2}\cdot E\left(k^2\right)\right]^2. \tag{15C}$$

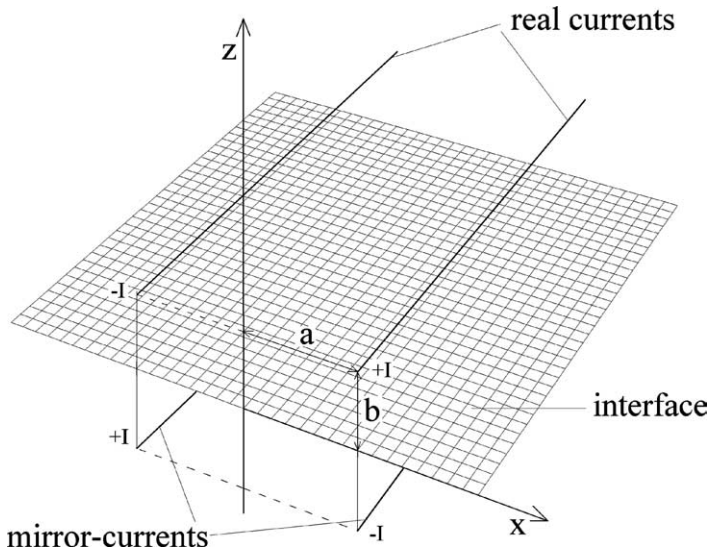

Fig. 3. Superposition of the magnetic field of the real currents and the imagined mirror-currents to deduce the magnetic field on the interface.

2.5. Drop shape in the absence of a magnetic field

We start the analysis with the case when the magnetic field is absent. The solution to this case was already derived by Laplace [15] and is needed to construct the Green's functions needed later on. Setting $\kappa_M = 0$, Eqs. (9) reduce to

$$h'' - Bo\,h = \kappa, \tag{16L}$$

$$h'' + \frac{1}{r}\,h' - Bo\,h = \kappa. \tag{16C}$$

It is convenient to represent the general solution to Eqs. (16) as the superposition of the general homogeneous solution h_H and the particular solution h_P, i.e.

$$h(x) = h_H(x) + h_P(x), \tag{17L}$$

$$h(r) = h_H(r) + h_P(r). \tag{17C}$$

We find

$$h_H(x) = C_1\cosh(\sqrt{Bo}\cdot x) + C_2\sinh(\sqrt{Bo}\cdot x), \tag{18L}$$

$$h_H(r) = C_1 I_0(\sqrt{Bo}\cdot r) + C_2 K_0(\sqrt{Bo}\cdot r), \tag{18C}$$

$$h_P = C_3 = -\frac{\kappa}{Bo}. \tag{19}$$

Substituting the boundary conditions given by Eqs. (13) into Eqs. (17), we obtain the constants

$$C_1 = -\frac{\tan\theta}{\sqrt{Bo}\sinh(\sqrt{Bo})}, \qquad C_2 = 0, \qquad C_3 = \frac{\tan\theta}{\sqrt{Bo}\tanh(\sqrt{Bo})}, \tag{20L}$$

$$C_1 = \frac{-\tan\theta}{\sqrt{Bo}\,I_1(\sqrt{Bo}\,R_C)}, \qquad C_2 = 0, \qquad C_3 = \frac{\tan\theta\cdot I_0(\sqrt{Bo}\,R_C)}{\sqrt{Bo}\,I_1(\sqrt{Bo}\,R_C)}. \tag{20C}$$

For the drop contour in the absence of the magnetic field we obtain

$$h(x) = \frac{\tan\theta}{\sqrt{Bo}\sinh(\sqrt{Bo})}\left[\cosh(\sqrt{Bo}) - \cosh(\sqrt{Bo}\,x)\right], \tag{21L}$$

$$h(r) = \frac{\tan\theta}{\sqrt{Bo}\,I_1(\sqrt{Bo})}\left[I_0(\sqrt{Bo}) - I_0(\sqrt{Bo}\,r)\right]. \tag{21C}$$

As obvious from Eqs. (19) and (20) the parameters κ, Bo and θ are interrelated according to

$$\kappa = -\frac{\sqrt{Bo}\tan\theta}{\tanh(\sqrt{Bo})}, \tag{22L}$$

$$\kappa = -\frac{\sqrt{Bo}\tan\theta\, I_0(\sqrt{Bo})}{I_1(\sqrt{Bo})}. \tag{22C}$$

2.6. Construction of Green's functions

A Green's function $G(x,\xi)$ or $G(r,\xi)$ describes the effect of a point disturbance in ξ on a differentially connected system (Duffy [17]). Outside this singular point the homogeneous solution of the problem is valid. These requirements allow us to construct the Green's functions G of the drop by solving the following differential equations:

$$G'' - Bo\,G = \delta(x-\xi), \tag{23L}$$

$$G'' + \frac{1}{r}G' - Bo\,G = \delta(r-\xi). \tag{23C}$$

The Green's functions are monotone over the whole interval $x = [0, L_C]$ and $r = [0, R_C]$, respectively, except for the position of the point disturbance, $x = \xi$ and $r = \xi$, respectively. Because of this singular behavior in ξ, we divide the function in a left part G_L and a right part G_R, see Fig. 4. The functions G_L and G_R must satisfy the conditions

$$\begin{aligned} &G_L(x=\xi) = G_R(x=\xi), \qquad G_R(x=L_C) = 0,\\ &G'_L(x=\xi) = G'_R(x=\xi) - 1, \end{aligned} \tag{24L}$$

$$\begin{aligned} &G_L(r=\xi) = G_R(r=\xi), \qquad G_R(r=R_C) = 0,\\ &G'_L(r=\xi) = G'_R(r=\xi) - 1. \end{aligned} \tag{24C}$$

The problem defined by Eqs. (23) and (24) yields the solutions

$$\begin{aligned} G_L(x,\xi) &= \frac{\cosh(\sqrt{Bo}\,x)\cdot\cosh(\sqrt{Bo}\,\xi)}{\sqrt{Bo}}\left[\tanh(\sqrt{Bo}\,\xi) - \tanh(\sqrt{Bo}\,L_C)\right],\\ G_R(x,\xi) &= \frac{\cosh(\sqrt{Bo}\,\xi)}{\sqrt{Bo}}\left[\sinh(\sqrt{Bo}\,x) - \tanh(\sqrt{Bo}\,L_C)\cdot\cosh(\sqrt{Bo}\,x)\right], \end{aligned} \tag{25L}$$

$$\begin{aligned} G_L(r,\xi) &= \xi\, I_0(\sqrt{Bo}\,r)\left[\frac{K_0(\sqrt{Bo}\,R_C)}{I_0(\sqrt{Bo}\,R_C)}\, I_0(\sqrt{Bo}\,\xi) - K_0(\sqrt{Bo}\,\xi)\right],\\ G_R(r,\xi) &= \xi\, I_0(\sqrt{Bo}\,\xi)\left[\frac{K_0(\sqrt{Bo}\,R_C)}{I_0(\sqrt{Bo}\,R_C)}\, I_0(\sqrt{Bo}\,r) - K_0(\sqrt{Bo}\,r)\right]. \end{aligned} \tag{25C}$$

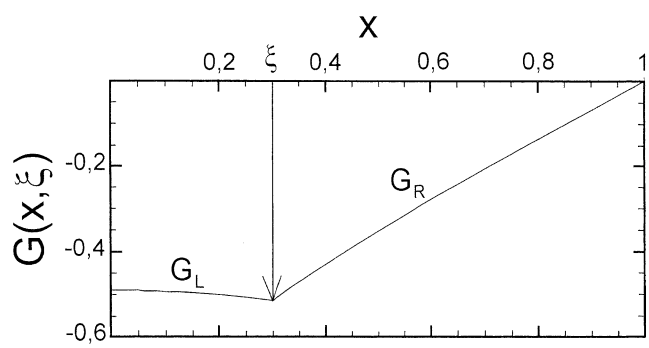

Fig. 4. Exemplary course of a Green's function of the long drop. The point of disturbance here lies at $\xi = 0.3$.

2.7. Drop shape in the presence of a magnetic field

Using the Green's functions defined above, the drop contour can be represented by the equations

$$h(x) = \int_0^x G_{\mathrm{R}}(x,\xi)\big[\kappa + \kappa_{\mathrm{M}} f_{\mathrm{M}}(\xi)\big]\,\mathrm{d}\xi + \int_x^{L_{\mathrm{C}}} G_{\mathrm{L}}(x,\xi)\big[\kappa + \kappa_{\mathrm{M}} f_{\mathrm{M}}(\xi)\big]\,\mathrm{d}\xi, \tag{26L}$$

$$h(r) = \int_0^r G_{\mathrm{R}}(r,\xi)\big[\kappa + \kappa_{\mathrm{M}} f_{\mathrm{M}}(\xi)\big]\,\mathrm{d}\xi + \int_r^{R_{\mathrm{C}}} G_{\mathrm{L}}(r,\xi)\big[\kappa + \kappa_{\mathrm{M}} f_{\mathrm{M}}(\xi)\big]\,\mathrm{d}\xi. \tag{26C}$$

As we shall see next, it is also necessary to determine the slope of the drop contour. It is given by the relations

$$h'(x) = \int_0^x G'_{\mathrm{R}}(x,\xi)\big[\kappa + \kappa_{\mathrm{M}} f_{\mathrm{M}}(\xi)\big]\,\mathrm{d}\xi + \int_x^{L_{\mathrm{C}}} G'_{\mathrm{L}}(x,\xi)\big[\kappa + \kappa_{\mathrm{M}} f_{\mathrm{M}}(\xi)\big]\,\mathrm{d}\xi, \tag{27L}$$

$$h'(r) = \int_0^r G'_{\mathrm{R}}(r,\xi)\big[\kappa + \kappa_{\mathrm{M}} f_{\mathrm{M}}(\xi)\big]\,\mathrm{d}\xi + \int_r^{R_{\mathrm{C}}} G'_{\mathrm{L}}(r,\xi)\big[\kappa + \kappa_{\mathrm{M}} f_{\mathrm{M}}(\xi)\big]\,\mathrm{d}\xi, \tag{27C}$$

where

$$\begin{aligned} G'_{\mathrm{L}}(x,\xi) &= \sinh(\sqrt{Bo}\,x)\cosh(\sqrt{Bo}\,\xi)\big[\tanh(\sqrt{Bo}\,\xi) - \tanh(\sqrt{Bo}\,L_{\mathrm{C}})\big], \\ G'_{\mathrm{R}}(x,\xi) &= \cosh(\sqrt{Bo}\,\xi)\big[\cosh(\sqrt{Bo}\,x) - \tanh(\sqrt{Bo}\,L_{\mathrm{C}})\sinh(\sqrt{Bo}\,x)\big], \end{aligned} \tag{28L}$$

$$\begin{aligned} G'_{\mathrm{L}}(r,\xi) &= \sqrt{Bo}\,\xi\, I_1(\sqrt{Bo}\,r)\left[\frac{K_0(\sqrt{Bo}\,R_{\mathrm{C}})}{I_0(\sqrt{Bo}\,R_{\mathrm{C}})}\, I_0(\sqrt{Bo}\,\xi) - K_0(\sqrt{Bo}\,\xi)\right], \\ G'_{\mathrm{R}}(r,\xi) &= \sqrt{Bo}\,\xi\, I_0(\sqrt{Bo}\,\xi)\left[\frac{K_0(\sqrt{Bo}\,R_{\mathrm{C}})}{I_0(\sqrt{Bo}\,R_{\mathrm{C}})}\, I_1(\sqrt{Bo}\,r) + K_1(\sqrt{Bo}\,r)\right]. \end{aligned} \tag{28C}$$

In the present case the inhomogeneity, given by the right-hand side of Eqs. (9), consists of two parts. The first part κ is constant (cf. Eqs. (22)). As discussed before, for a constant Bond number, the parameter κ determines the contact angle θ which is fixed in the present analysis. However, the second part, $\kappa_{\mathrm{M}} f_{\mathrm{I}}(x)$ and $\kappa_{\mathrm{M}} f_{\mathrm{I}}(r)$, which is related to the magnetic pressure, alters the original contact angle. The value of this alteration is given by (cf. Eqs. (27))

$$\tan\theta_{\mathrm{M}}(x = L_{\mathrm{C}}) = \int_0^{L_{\mathrm{C}}} G'_{\mathrm{R}}(x = L_{\mathrm{C}}, \xi)\kappa_{\mathrm{M}} f_{\mathrm{M}}(x = \xi)\,\mathrm{d}\xi, \tag{29L}$$

$$\tan\theta_{\mathrm{M}}(r = R_{\mathrm{C}}) = \int_0^{R_{\mathrm{C}}} G'_{\mathrm{R}}(r = R_{\mathrm{C}}, \xi)\kappa_{\mathrm{M}} f_{\mathrm{M}}(r = \xi)\,\mathrm{d}\xi. \tag{29C}$$

Therefore, to reinstate the fixed contact angle we have to correct the analysis by exactly this value. Finally, we calculate the drop contour by evaluating the relations

$$\begin{aligned} h(x) \;=\; & \int_0^x G_{\mathrm{R}}(x,\xi)\left[\frac{\sqrt{Bo}}{\tanh(\sqrt{Bo})}(\tan\theta_{\mathrm{M}} - \tan\theta) + \kappa_{\mathrm{M}} f_{\mathrm{M}}(\xi)\right]\mathrm{d}\xi \\ & + \int_x^{L_{\mathrm{C}}} G_{\mathrm{L}}(x,\xi)\left[\frac{\sqrt{Bo}}{\tanh(\sqrt{Bo})}(\tan\theta_{\mathrm{M}} - \tan\theta) + \kappa_{\mathrm{M}} f_{\mathrm{M}}(\xi)\right]\mathrm{d}\xi, \end{aligned} \tag{30L}$$

$$h(r) = \int_0^r G_{\mathrm{R}}(r,\xi)\left[\frac{\sqrt{Bo}\,I_0(\sqrt{Bo})}{I_1(\sqrt{Bo})}(\tan\theta_{\mathrm{M}} - \tan\theta) + \kappa_{\mathrm{M}} f_{\mathrm{M}}(\xi)\right]\mathrm{d}\xi + \int_r^{R_{\mathrm{C}}} G_{\mathrm{L}}(r,\xi)\left[\frac{\sqrt{Bo}\,I_0(\sqrt{Bo})}{I_1(\sqrt{Bo})}(\tan\theta_{\mathrm{M}} - \tan\theta) + \kappa_{\mathrm{M}} f_{\mathrm{M}}(\xi)\right]\mathrm{d}\xi. \tag{30C}$$

The drop volume can be calculated using the relations

$$V = \int_0^{L_{\mathrm{C}}} h(x)\,\mathrm{d}x, \tag{31L}$$

$$V = 2\pi \int_0^{R_{\mathrm{C}}} r h(r)\,\mathrm{d}r. \tag{31C}$$

Summarizing our theoretical model, we use the flat drop approximation to simplify the governing Young–Laplace equation. The skin depth approximation enables us to include the magnetic pressure into this equation. The effect of the magnetic field is represented by an integral sum of point disturbances. The drop contours are then obtained analytically by applying the Green's function theory. A correction is made to restore the fixed contact angle. The integration of these corrected contours determines the drop volume.

3. Results and discussion

When solving Eqs. (30), there are three main questions we want to address. First, assuming conserved volume, how will the drop be squeezed when submitted to a magnetic field? Second, which amount of fluid can be supported within the inductor dimensions at different magnetic field intensities? And third, how is the drop shaped when pumped up in given magnetic field? In the following we show results of drop contours for a fixed contact angle of $\theta = 30°$ and a fixed horizontal position of the inductor at $a = 1$. The results are discussed while varying the Bond number and the magnetic pressure ratio. Moreover, results for two different vertical inductor positions, b, are presented.

3.1. Squeezing

In this section we consider the case when a drop of fixed volume is squeezed using a high-frequency magnetic field. This case is important in applications concerning the electromagnetic shaping of a liquid metal dome. During the squeezing process, we increase the magnetic pressure ratio κ_{M} while inductor position and Bond number remain unchanged. The drop volume is calculated in the case $\kappa_{\mathrm{M}} = 0$ when the magnetic field is absent and the contact is at $L_{\mathrm{C0}} = 1$ and $R_{\mathrm{C0}} = 1$, respectively. For $\kappa_{\mathrm{M}} \neq 0$ we first use Eqs. (31) to graphically determine the changed contact positions L_{C} and R_{C} at the given volume. Inserting these new contact positions into Eqs. (30) leads to the desired drop contours. The pictures in Figs. 5 and 6 show the resulting shapes of a long drop and a circular drop, respectively, when magnetically squeezed from $\kappa_{\mathrm{M}} = 0$ to $\kappa_{\mathrm{M}} = 10$ in equidistant steps. Fig. 5(a) refers to a long drop and a Bond number of $Bo = 100$, squeezed by an inductor located at $b = 0.5$. The induced magnetic pressure is highest at the contact line and decreases to zero at $x = 0$. Therefore, when the magnetic field is intensified, the growing pressure near the contact line must be balanced by an elevation of the drop in the center. Because of the volume conservation, the position of the contact line moves toward the center. The drop is squeezed. For instance, when $\kappa_{\mathrm{M}} = 10$, the original contact length is nearly halved while the drop height in the center is more than doubled. However, due to the squeezing, the inductor loses its effectiveness as its distance to the contact line increases. In Fig. 5(a) this can be seen by the slowing down of the squeezing at higher values of κ_{M}.

Considering the squeezing of a circular drop in Fig. 6(a), we observe a definite difference. Here, at $\kappa_{\mathrm{M}} = 10$, the drop mounts up to almost four times the original height. This contrast arises from the geometrical differences. In the circular geometry we have a concentric distribution of the magnetic isolines. Hence, the pressure on the drop border has more surface to act on and causes a higher elevation of the fluid in the center. A comparison of the contour plots in Figs. 5(a)–(b) and 6(a)–(b), respectively, illustrates the effect of increasing the inductor distance from $b = 0.5$ to $b = 1$. As expected, the squeezing effect is diminished when the inductor is arranged at a larger distance from the interface. A comparison of the contour plots given in Figs. 5(b)–(d) shows the effect of decreasing the Bond number from $Bo = 100$ to $Bo = 10$ and $Bo = 1$. According to Eqs. (10), at constant material properties, a decrease of the Bond number corresponds to a decrease of the drop volume. As Figs. 5 show, for smaller

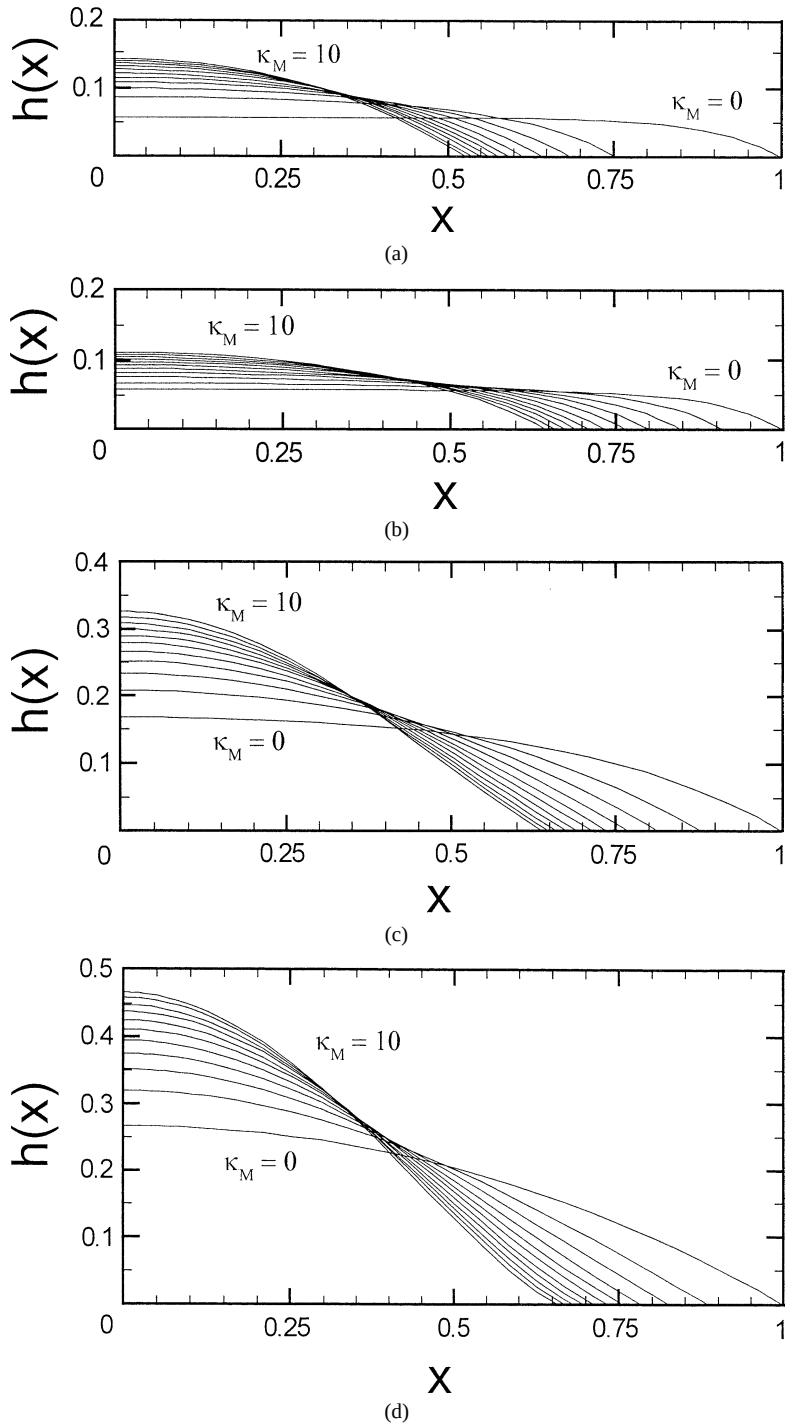

Fig. 5. Squeezing of long drops. The magnetic pressure ratio varies from $\kappa_M = 0$ to $\kappa_M = 10$ and is increased in constant increments. Hereby the drop volume is fixed as well as the contact angle, i.e. $\theta = 30°$. The horizontal inductor position is $a = 1$. Bond number and inductor height are varied as follows. (a) $Bo = 100$, $b = 0.5$, (b) $Bo = 100$, $b = 1$, (c) $Bo = 10$, $b = 1$, (d) $Bo = 1$, $b = 1$.

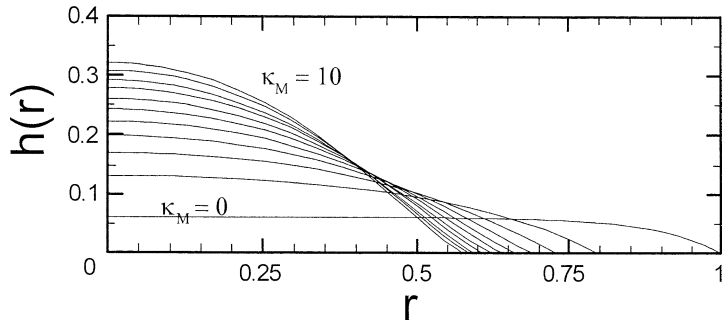

(a)

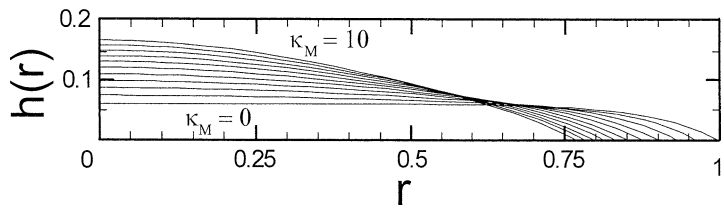

(b)

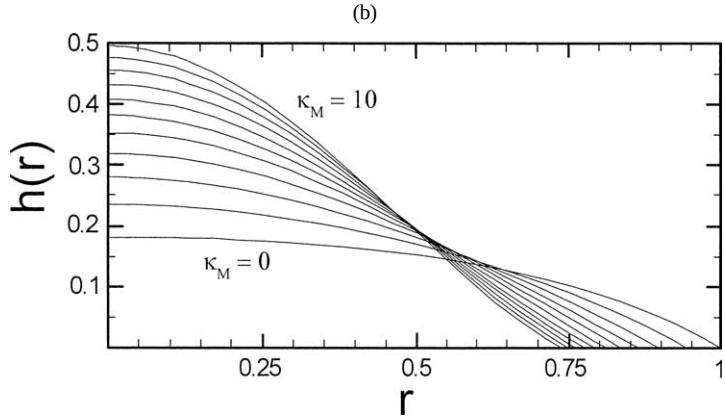

(c)

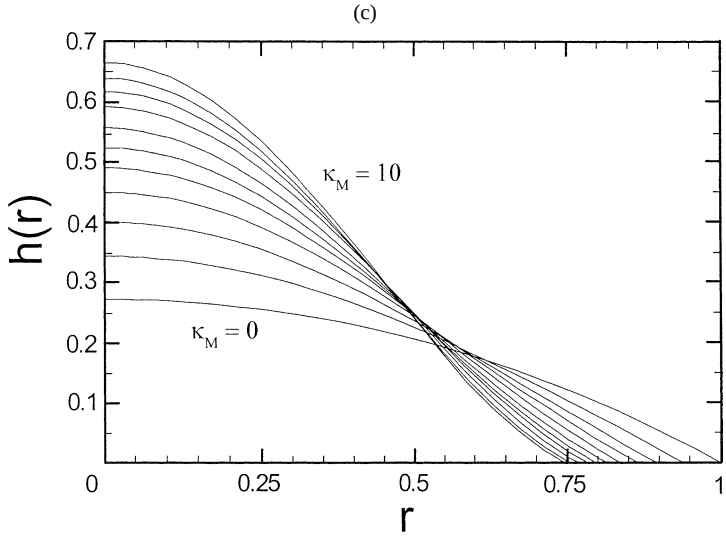

(d)

Fig. 6. Squeezing of circular drops. The magnetic pressure ratio varies from $\kappa_M = 0$ to $\kappa_M = 10$ and is increased in constant increments. Hereby the drop volume is fixed as well as the contact angle, i.e. $\theta = 30°$. The horizontal inductor position is $a = 1$. Bond number and inductor height are varied as follows. (a) $Bo = 100$, $b = 0.5$, (b) $Bo = 100$, $b = 1$, (c) $Bo = 10$, $b = 1$, (c) $Bo = 1$, $b = 1$.

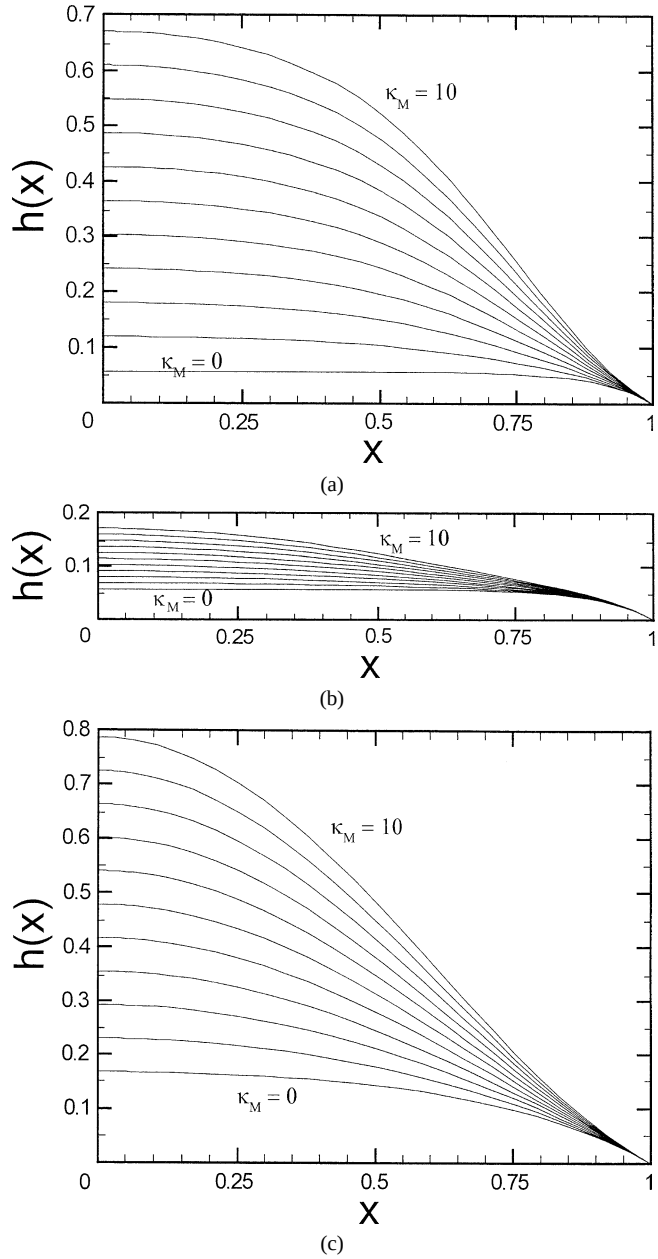

Fig. 7. Supporting of long drops. The effects of Bond number and inductor height are shown. Thereby the contact position is pinned. The magnetic pressure ratio varies from $\kappa_M = 0$ to $\kappa_M = 10$ and is increased in constant increments, the contact angle remains constant, i.e. $\theta = 30°$. The horizontal inductor position is $a = 1$. The corresponding Bond numbers and inductor heights are (a) $Bo = 100$, $b = 0.5$, (b) $Bo = 100$, $b = 1$, (c) $Bo = 10$, $b = 1$, (d) $Bo = 1$, $b = 1$.

Bond numbers the drop shape becomes more hemispherical. This can be explained by the fact that for smaller drops the surface tension effects are dominant. However, the relative squeezing effect of the magnetic field on the drop is nearly independent of the Bond number. For a given value of the magnetic pressure ratio κ_M, the position of contact does not change upon decreasing *Bo*. We conclude that this result is due to the assumption of a fixed contact angle favouring geometrically similar shapes.

3.2. Supporting

We discuss next the case of drops with a fixed contact position at $L_C = 1$ and $R_C = 1$, respectively. In application, the contact position may be pinned by the solid material below. Consequently, to meet this condition, for a different value of the

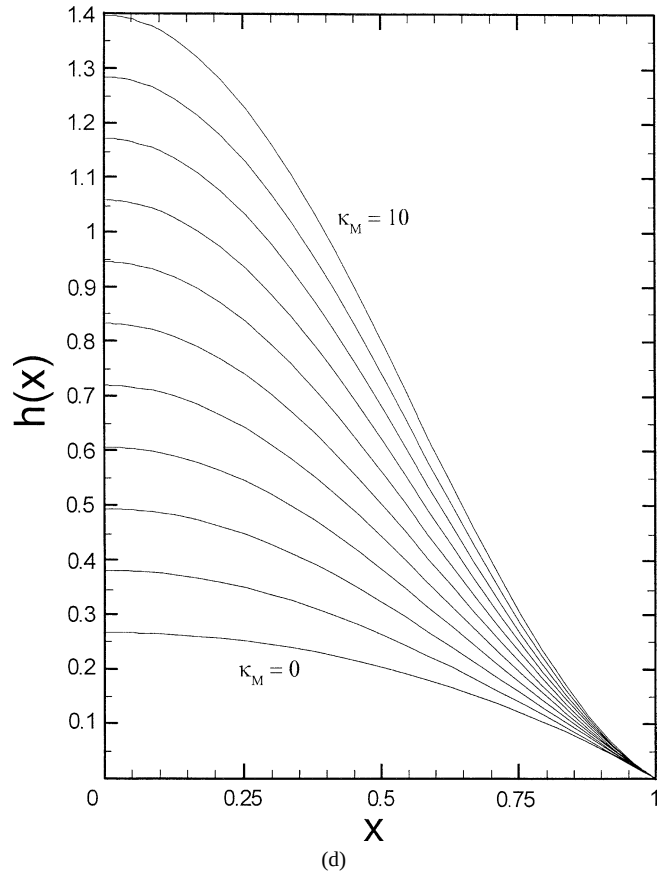

(d)

Fig. 7. (continued).

parameter κ_M each contour confines a different volume that can be supported by the magnetic field. In this case we can calculate the contours directly using Eqs. (30). The results are shown in Figs. 7 for the long drop and in Figs. 8 for the circular drop, respectively. We start the discussion with the long drop with a Bond number $Bo = 100$ and an inductor position $b = 0.5$ cf. Fig. 7(a). Upon increasing the parameter κ_M we see a clear increase of the drop volume that can be supported by the magnetic field. For instance, at a magnetic pressure ratio of $\kappa_M = 10$, the supported drop volume increases by a factor of 8 compared to the case when the magnetic field is absent. However, it should be mentioned that at such high values of κ_M, the resulting drop shapes are not in agreement with our basic assumptions, i.e. $h' \ll 1$ and $h(0)/b \ll 1$. Therefore, the shown results may demonstrate only qualitatively that originally flat drops can be deformed electromagnetically into a nearly hemispherical shape. Fig. 7(b) shows the supporting of drops at parameter values fixed at $b = 1$ and $Bo = 100$. As expected, upon doubling the distance between inductor and drop surface, the supporting effect decreases. In detail, $\kappa_M = 10$ we find that the supported drop volume increases only by a factor of 2 compared to the case $\kappa_M = 0$. This quantitative result agrees well with the physical fact that the magnetic induction on the drop surface decays according to $B \propto 1/b$. The induced magnetic pressure decays according to $p_M \propto 1/b^2$. Figs. 7(b)–(d) demonstrate the effects of decreasing the Bond number from $Bo = 100$ (Fig. 7(b)) to $Bo = 10$ (Fig. 7(c)) and $Bo = 1$ (Fig. 7(d)) at a constant value of b, i.e. $b = 1$. As it can be seen, the drop volume that can be supported increases as the Bond number is decreased. According to Eqs. (10), this can be explained by the reduction of the action of gravity against which the drop must be deformed. Another special feature shown in Figs. 7 is that, in the present case of a fixed contact position, an increase of the magnetic pressure ratio κ_M results in a corresponding increase of the drop height in the center. This is due to the fact that the induced effective magnetic pressure is not weakened by a movement of the contact line. Thus, the magnetic pressure can balance completely the hydrostatic pressure rise. The corresponding results for circular drops are shown in Fig. 8(a)–(d). We observe the same effects as discussed above. Quantitative differences can be explained by the geometrical differences mentioned before.

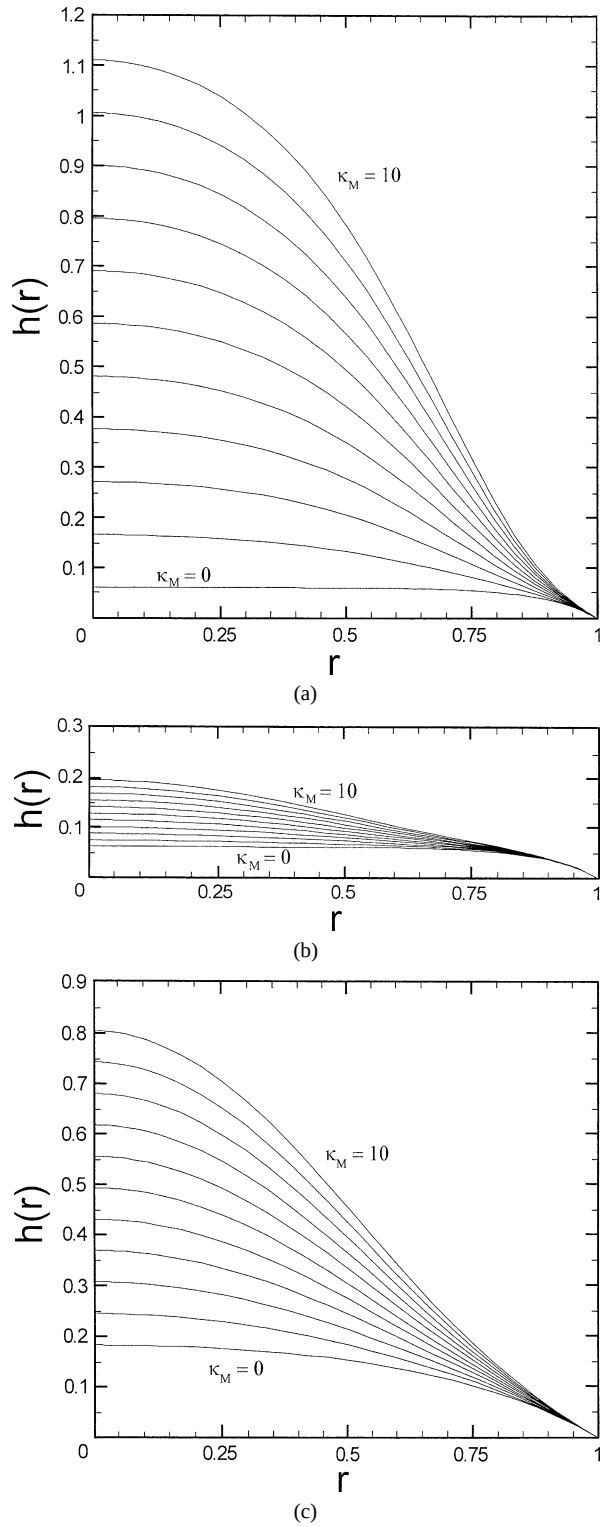

Fig. 8. Supporting of circular drops. The effects of Bond number and inductor height are shown. Thereby the contact position is pinned. The magnetic pressure ratio varies from $\kappa_M = 0$ to $\kappa_M = 10$ and is increased in constant increments, the contact angle remains constant, i.e. $\theta = 30°$. The horizontal inductor position is $a = 1$. The corresponding Bond numbers and inductor heights are (a) $Bo = 100$, $b = 0.5$, (b) $Bo = 100$, $b = 1$, (c) $Bo = 10$, $b = 1$, (d) $Bo = 1$, $b = 1$.

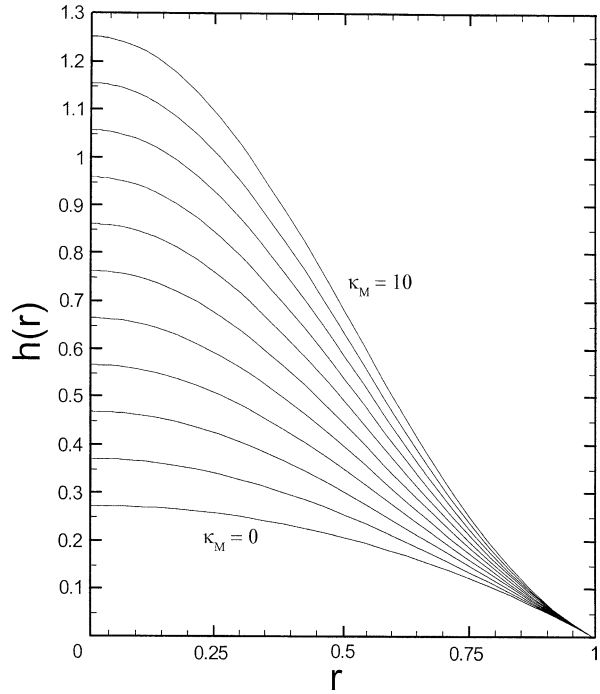

Fig. 8. (continued.)

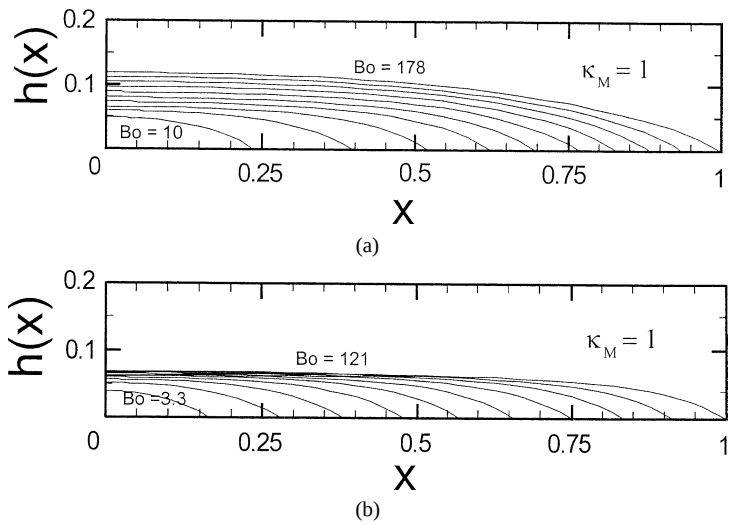

Fig. 9. Pumping up of long drops. The magnetic pressure ratio remains constant at $\kappa_M = 1$ while the drop is inflated. The drop volume is increased in 10 constant steps. Therefore, also the Bond number rises. We suppose the contact angle to stay constant at $\theta = 30°$, the horizontal inductor position be $a = 1$. The vertical inductor positions are (a) $b = 0.5$, (b) $b = 1$.

3.3. Pumping up

Finally, we calculate the static shape of drops of different Bond numbers in a given magnetic field, i.e. $\kappa_M = 1$ being constant, while the contact position is free to move. According to Eqs. (10), the alteration of the Bond number is related to an alteration of the drop volume. Thus, the present case corresponds to a pumping up.

Using Eqs. (31) we first calculate the volume V_1 of a drop with contact position at $L_{C1} = 1$ and $R_{C1} = 1$ for a given Bond number Bo_1 and $\kappa_M = 1$. We divide this volume in 10 portions and determine the corresponding contact positions. Inserting

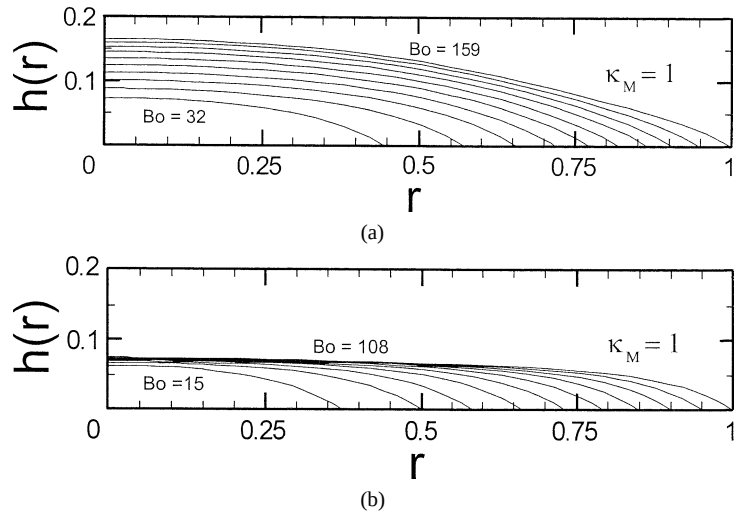

Fig. 10. Pumping up of circular drops. The magnetic pressure ratio remains constant at $\kappa_M = 1$ while the drop is inflated. The drop volume is increased in 10 constant steps. Therefore, also the Bond number rises. We suppose the contact angle to stay constant at $\theta = 30°$, the horizontal inductor position be $a = 1$. The vertical inductor positions are (a) $b = 0.5$, (b) $b = 1$.

these contact positions into Eqs. (30) leads to the contours shown in Figs. 9(a)–(b) for the long drop and Figs. 10(a)–(b) for the circular drop. Mathematically, this calculation method corresponds to a rescaling of the coordinates according to $x, h(x) \propto L_{C1}$ and $r, h(r) \propto R_{C1}$, respectively. Fig. 9(a) shows the result when the inductor is arranged at $b = 0.5$. We find that, in the beginning of the pumping up ($Bo = 10$), the drop shape is more round. Again, this is explained by the higher influence of surface tension at small drop volumes. As the drop volume and thus the Bond number is increased, the drop spreads laterally. Therefore, the distance to the inductor decreases and the support by the magnetic field increases. By that the drop height in the center likewise increases. Fig. 9(b) show the inflated drop contours for the case $b = 1$. As expected, upon doubling the distance between drop and inductor, the supporting effect of the magnetic field is clearly diminished. As the Bond number is increased, the drop remains almost flat while spreading. Compared to the case $b = 0.5$, the supported volume of the fully inflated drop is reduced by a factor of 2. The corresponding results for circular drops are shown in Figs. 10(a)–(b). The effects of the magnetic field are similar to the long drop arrangement and differ only due to the change of geometry.

4. Summary

We have presented an analytical model to calculate the static shape of metal drops affected by a high-frequency magnetic field. We have supplemented the Young–Laplace equation with a magnetic pressure term that represents the induced Lorentz forces within the drop in the limit of vanishing skin depth. The problem is simplified by applying the thin drop approximation and using the mirror image method to calculate the magnetic pressure. We use Green's function techniques to solve for the drop shape. Three possible applications are of interest:

First, the squeezing of a drop of constant volume to form a molten metal dome in cold crucible applications. Second, the supporting of drops of different volume in a given magnetic field, which is important for semi-levitation devices. And third, the pumping up of a drop is relevant in application because the static drop shapes of the two former cases first have to grow into their final dimensions. In all cases we have found high-frequency magnetic fields to be a promising tool for electromagnetic shaping of free surfaces. Shapes which are almost hemispherical can be formed and supported. However, it is necessary to keep in mind that the shapes may tend to be unstable, as the experiments mentioned in the introduction indicate. For a final conclusion about the practical applicability, a supplementary stability theory is needed.

Acknowledgements

The investigation presented was performed within the framework of the "Forschergruppe Magnetofluiddynamik" and sponsored by the Deutsche Forschungsgemeinschaft (DFG) under grant FOR 421/1-2 Ka-A4. We would like to thank Professors A. Thess and P.H. Steen for interesting discussions. We are grateful for the advices given by Professor Fautrelle and Dr.

Molokov. Furthermore, we acknowledge financial support by the Deutscher Akademischer Austauschdienst (DAAD) within the PROCOPE program under grant. D/0333638.

References

[1] P.A. Davidson, An Introduction to Magnetohydrodynamics, Cambridge University Press, 2001.
[2] H. Tanado, K. Tainuma, T. Take, T. Shinokura, S. Hayashi, Vacuum melting with cold crucible levitation melting furnaces, in: Proceedings of the 3rd International Symposium on Electromagnetic Processing of Materials, Nagoya, Japan, April 3–6, 2000, pp. 277–282.
[3] E. Takeuchi, K. Miyazawa, Electromagnetic casting technology of steel, in: Proceedings of the 3rd International Symposium on Electromagnetic Processing of Materials, Nagoya, Japan, April 3–6, 2000, pp. 20–27.
[4] J.W. Evans, D. Prasso, D. Gupta, R. Kageyama, Electromagnetic casting (Modeling of heat transport and surface instability), Magnetohydrodynamics 32 (2) (1996) 142–147.
[5] V. Kocourek, M. Conrath, Ch. Karcher, Shaping of a liquid metal drop using high-frequency magnetic fields, in: Fifth International Pamir Conference on Fundamental and Applied MHD, vol. 1, Ramatuelle, France, 2002, pp. 199–204.
[6] S. Molokov, C.B. Reed, Fully developed magnetohydrodynamic flow in a rivulet, ANL Report No. ANL/TD/TM00-12, Argonne, 2000.
[7] Y. Fautrelle, J. Etay, S. Daugan, Free surface horizontal waves generated by low frequency alternating magnetic fields, Fluid Flow Phenomena in Metals Processing, San Diego, 1999.
[8] L.D. Landau, E.M. Lifschitz, Course of Theoretical Physics. Vol. 6. Hydrodynamics, second ed., Pergamon Press, Oxford, 2000.
[9] J.D. Jackson, Classical Electrodynamics, third ed., Wiley, 1999.
[10] D.N. Riahi, J.S. Walker, Float zone shape and stability with the electromagnetic body force due to a radio frequency induction coil, J. Crystal Growth 94 (1989) 635–642.
[11] K.H. Lie, J.S. Walker, D.N. Riahi, Free surface shape and AC electric current distribution for float zone silicon growth with a radio frequency induction coil, J. Crystal Growth 100 (1990) 450–458.
[12] V. Kocourek, M. Conrath, On the stability of liquid metal drops affected by high-frequency magnetic fields, Private communication, Preprint for submission to Phys. Rev. Lett., October 2003.
[13] R. Moreau, Magnetohydrodynamics, Kluwer Academic, 1990.
[14] T. Young, An essay on the cohesion of fluids, Philos. Trans. Roy. Soc. London 94 (1805) 65–87.
[15] P.S. de Laplace (Marquis), Traité de Mécanique Céleste. 4th volume, 1st section (thérorie de l'action capillaire) of the supplement to book 10 (sur divers points relatifs au système du monde). Published by Chez Courier, Paris, 1805.
[16] W.R. Smythe, Static and Dynamic Electricity, third ed., Taylor & Francis, 1989.
[17] D.G. Duffy, Green's Functions with Applications, Chapman & Hall/CRC, 2001.